Journal of
Ceramic Science
and Technology

J. Ceram. Sci. Tech., **06** [04] 329-338 (2015)
DOI: 10.4416/JCST2015-00062
available online at: http://www.ceramic-science.com

3D Focalization Microfluidic Device Built with LTCC Technology for Nanoparticle Generation using Nanoprecipitation Route

H.C. Gomez[1], M.R. Gongora-Rubio[*2], B.O. Agio[2], J. de Novais Schianti[2], V. Tiemi Kimura[2], A- Marim de Oliveira[2], L. Wasnievski da Silva de Luca Ramos[2], A.C. Seabra[1]

[1]Escola Politécnica da Universidade de São Paulo (USP), Laboratório de Sistemas Integráveis, Av. Prof. Luciano Gualberto, 158, 05508 – 900, São Paulo, Brasil
[2]Instituto de Pesquisas Tecnológicas do Estado de São Paulo (IPT), Núcleo de Bionanomanufatura, Av. Prof. Almeida prado, 532, 05508-901, São Paulo, Brasil
received September 18, 2015; received in revised form November 11, 2015; accepted November 25, 2015

Abstract

Nanoprecipitation is a nanonization technique used for generating nanoparticles. Fields like pharmaceuticals and fine chemistry make use of such techniques. Typically, bulky batch mechanical processes are used, but these result in a high polydispersity index of the generated nanoparticles, poor particle size reproducibility and energy waste.

LTCC-based microsystem technologies allow the implementation of different unitary operations for the chemical process, making it an enabling technology for miniaturization. In fact, LTCC microfluidic reactors have recently been used to produce micro- and nanoparticles with excellent control of size distribution and morphology.

The present work reports on the performance of two 3D LTCC flow-focusing microfluidic devices designed to fabricate polymeric nanocapsules for hydrocortisone acetate drug encapsulation, based on the nanoprecipitation route. Monomodal submicron and nanometer particles were obtained. Zetasizer-measured sizes (Tp) were in the range from 162.2 nm to 459.1 nm with a polydispersity index (PDI) ranging from 0.102 to 0.235.

Keywords: Nanoprecipitation, fluid flow focusing, LTCC, nanoparticles.

I. Introduction

Nanoprecipitation is a nanonization technique used for nanoparticle generation in a number of fields such as drug formulation and chemistry [1–6]. With this strategy, an organic solution, which is made up of dissolved materials (polymers and pharmaceutical actives), is placed in contact with an antisolvent flow. High material concentration regions are created owing to diffusion of the solvent from organic phase into the antisolvent flow. In these regions, the material is no longer soluble in the solvent-antisolvent mixture, increasing its concentration. When a material concentration exceeds a critical level, spontaneous nucleation takes place, generating nanoparticles.

In order to find the regions in which nanoprecipitation takes place, it is interesting to know the solubility parameters of the materials and solvent-antisolvent mixture and compare them. An element is perfectly dissolved by a solvent when the solubility parameters of the element and solvent match [7–10]. Hansen divided the solubility parameters into three individual parameters called Hansen Solubility Parameters (HSP). "The basis of these so-called HSPs is that the total energy of vaporization ... consists of several individual parts. These arise from (atomic) dispersion forces (δ_d), (molecular) permanent dipole-permanent dipole forces (δ_p), and (molecular) hydrogen bonding (electron exchange) (δ_h)" [8]. A Hansen Solubility Sphere (HSS) defines a region in a three-dimensional space (δ_d, δ_p, δ_h), centered in the element's HSPs. All solvents with HSPs inside this region are considered good solvents for that element [8–11]. The regions at which the HSPs of a solvent-antisolvent mixture start falling outside the HSS are considered as places of nanoparticle generation [12].

Several works have reported the use of microfluidics devices in nanoprecipitation. They mainly make use of topologies with Y-junction shape [13–17] or T-junction shape with central channel for the organic dissolved material, and two antisolvent input channels with 180° angle [4,18,19] or lower [20–23]. The operating principle of the Y-junction shape is based on solvent diffusion through a single solvent-antisolvent fluid interface. The diffusion profile and fluid interface can be seen in Fig. 1a. The T-junction has two solvent-antisolvent fluid interfaces because of the antisolvent stream focalization effect, which improves the total diffusion process and hence the nanoprecipitation process, Fig. 1b. For this work, T-junction shapes are referred to as 2D flow focalization because all contact interfaces formed between the solvent and antisolvent flows are almost planar. Devices like this lose their focalization effect when the ratio of the antisolvent to solvent flow rates exceeds a certain value.

* Corresponding author: gongoram@ipt.br

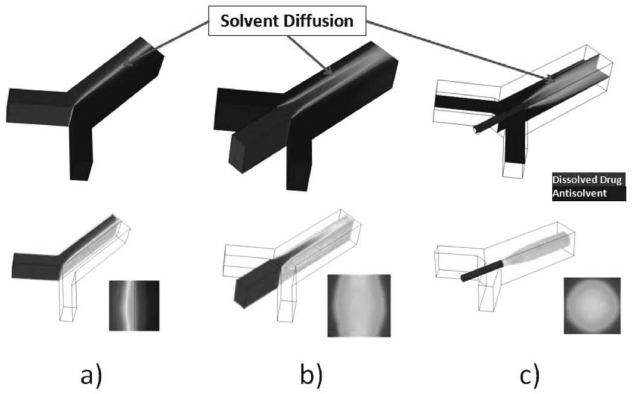

Fig. 1: Solvent diffusion into antisolvent fluid using different microfluidic topologies. a) Y-junction shape, single-flow interface. b) T-junction with central channel for solvent fluid and antisolvent inputs' angle lower than 180° (2D flow focalization), two-flow interface. c) 3D flow focalization device, 360° flow interface.

The diffusion process can also be improved by having the solvent stream surrounded by the antisolvent stream. This technique is referred to as 3D flow focalization [24–28], Fig. 1c. In this approach, the dissolved material stream does not wet the channel walls, which is not the case in examples of previous devices. This can also be useful in order to prevent clogging of the channel when hydrophobic materials are processed with water being used as an antisolvent [24].

Different substrates and techniques have been used for the fabrication of microfluidic devices. Polymers like polymethylmethacrylate (PMMA) and poly(dimethylsiloxane) (PDMS) have been used as a substrate in a standard micromolding process [13, 18, 19, 24, 25, 27]. Glass has also been used as a substrate using standard photolithographic and wet etching procedures [20–22]. Low Temperature Co-fired Ceramics (LTCC) is another substrate used [23, 26, 28]. Compared with the previously mentioned materials, LTCC exhibits interesting advantages such as the possibility to microfabricate 3D geometries, chemical inertness to most solvents, low contact angle, low coefficient of thermal expansion, stability in high operational temperatures as well as resistance to high internal pressures, allowing the implementation of several chemical processes with applications in extreme environments.

Glass and polymer microfluidic devices cannot withstand high channel pressures owing to the fragility of the glass and swelling of the polymer channels. Because of this, the flow rate in these systems is limited to a few tens or hundred μl/min. Owing to the high internal pressures the LTCC substrate is able to resist, the flow rate can be increased to hundreds ml/min, which is beneficial for production scale-up.

This work shows a 3D microfluidic flow focalization device manufactured with LTCC technology for use in a nanoprecipitation process. The proposed geometries are designed to improve the solvent diffusion process by surrounding the organic phase with antisolvent fluid flow. This research is still in progress, here initial simulations and operating results of a nanoprecipitation device used for polymeric nanoencapsulation of a hydrocortisone acetate drug are presented.

II. Device Layout

Two devices were fabricated and tested. The main difference is the configuration of the input channels. The layout of the devices is presented in Fig. 2. They are formed based on three fundamental blocks. These are the input of the organic phase dissolved material (DM), the input of the antisolvent (AS) and the nanoprecipitation channel (NPC). The DM input is centered in the NPC.

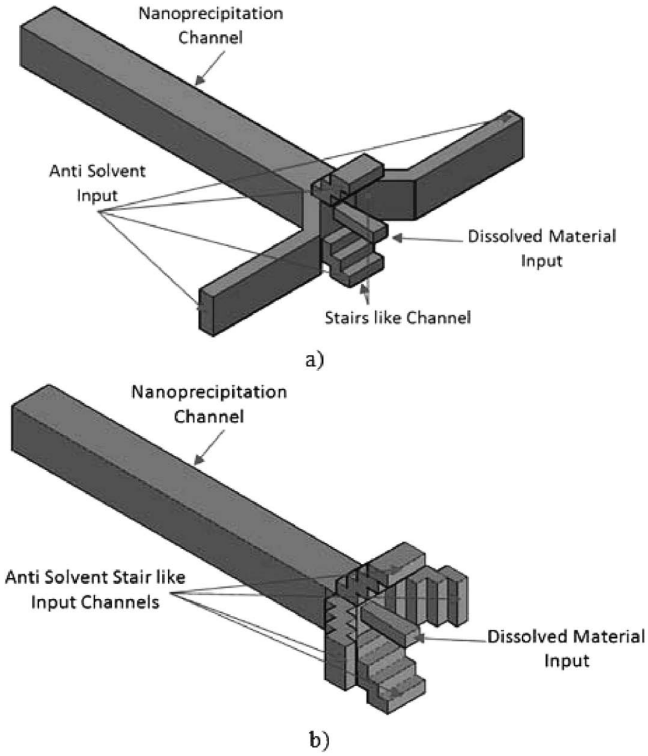

Fig. 2: 3D focalization microfluidic devices. Antisolvent inputs with stair-like channels. a) Device 1 (D1NSI) with non-symmetric antisolvent inputs. b) Device 2 (D2SI) with symmetric antisolvent input.

For both devices, the NPC design dimensions were 0.781 x 6.5 x 0.772 mm (w x l x h) corresponding to D_H = 776 μm. The DM input design dimensions were 0.217 x 0.214 mm (w x h), corresponding to D_H = 216 μm.

In accordance with the datasheet provided by the manufacturer of the green ceramic tape, shrinkage after sintering of 13 % in the x-y axis and 15.5 % in the z axis can be expected. This information must be taken into account at the design stage. For this reason, the CAD files for the NPC and DM input were dimensioned as follows:

- NPC: 0.8974 x 7.47 x 0.914 mm (w x l x h),
- DM input: 0.2494 x 0.254 mm (w x h)

The four AS inputs have an input angle of 45° to the NPC direction. For Device 1 (D1NSI), Fig. 2a, this angle is assured with stair-like channels (fabrication constraint) in the vertical direction. Owing to the difference in the topology of the AS channels in the vertical and horizontal directions, AS input fluid asymmetries can be expected. For this reason, Device 2 (D2SI), Fig. 2b, was manufactured with all AS input channels with the same topology, taking into account the vertical fabrication constraint.

The configuration of the AS channels will force the DM to be focalized in the center of the NPC along the device.

This is due to the AS flow force action on the central DM flow, inducing a cylindrical flow stream.

III. Materials and Method

(1) Manufacturing process

Fabrication of the microfluidic devices employed the typical LTCC process [29]. Dupont 951P2 and 951PX green LTCC ceramic tapes were used. Layers were fabricated using a prototyping machine equipped with an ultraviolet laser (355-nm wavelength), model LPKF Protolaser U3 (LPKFLaser & Electronics AG). A one-step thermo-compression lamination process was performed by means of a uniaxial laminator with pressure of 11.8 MPa at 70 °C (hydraulic press machine, model MA098/A30, Marconi). Prior to the lamination process, the aligned sheets were baked at 60 °C for 20 min. For sintering, a muffle furnace (EDG Equipment, model EDG10P-S) was used, with a two-stage profile: first, heating of the device at 450 °C for 30 min followed by sintering at 850 °C for 60 min. The temperature ramps in the furnace were programmed with a slope of 10 °C/min.

The input and output brass fluidic interconnection tubes were glued to the ceramics using a high-temperature epoxy (EPO-TEK 353ND). The gluing process was performed with a hot plate at 150 °C for 2 min.

The sintered devices were externally measured in order to determine the real shrinkage. It was verified that device D1NSI experienced x-y and z shrinkage of 13.6 % and 21.7 % respectively. So, for this device the real dimensions were:

- NPC: 0.775 x 6.45 x 0.716 mm (w x l x h) (DH = 744 µm)
- DM input: 0.215 x 0.199 mm (wxh) (DH = 207µm)

Device D2SI experienced x-y and z shrinkage of 12.2 % and 18.3 % respectively. The real dimensions were:

- NPC: 0.788 x 6.56 x 0.747 mm (w x l x h) (DH = 767 µm)
- DM input: 0.219 x 0.207 mm (w x h) (DH = 213 µm)

The fabricated device is depicted in Fig. 3, showing the two material inlets and the nanoparticle outlet.

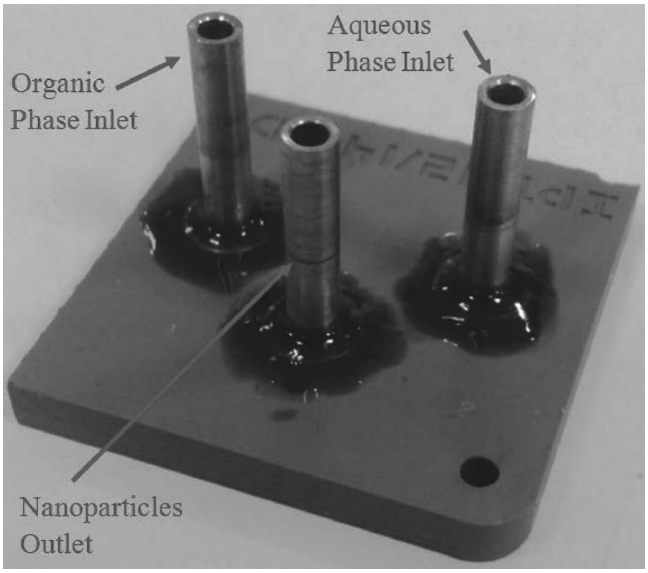

Fig. 3: Fabricated LTCC device.

(2) Sample preparation

The material dissolved in organic phase fluid was prepared from 1 g of a homemade block copolymer (PCL 80K -Pluronic F127) [30] and 100 mg hydrocortisone acetate and mixed in 20 ml acetone (Sigma Aldrich) until completely dissolved.

As antisolvent fluid material, 100 ml purified DI water was used. A Milli-Q system (Millipore Corporation, USA) was employed to obtain the purified water.

(3) Size measurement

For measuring the diameter of the particles, a Zetasizer Nano-ZS (Mo.: ZEN3600, Malvern Instruments Limited) was used.

(4) Pumping system

Two syringe pumps (PHD 4400, Harvard Apparatus) [31] were used to pump the DM and AS into the microfluidic device.

(5) Simulation and processing software

COMSOL® Multiphysics software was used for evaluation of the acetone diffusion profile and the devices.

Statistica12® software was used for analyzing the simulation and experimental results.

(6) Experimental design

A factorial experimental planning approach was applied to validate the D1NSI and D2SI performance and to verify the nanoparticles' size variation as a function of the process variables [32]. Two operational parameters, Flow Rate Ratio (R_Q) and Total Flow Rate (Q_T), as shown in Table 1, were analyzed, totaling four experiments (for conditions -1 and 1). For D2SI, a central point was also analyzed and repeated three times. For D1NSI, an additional experiment was performed for testing the function of the device with an intermediate process variable value.

Table 1: Experiment configuration.

Process Variables	Experiment Conditions					Intermediate value
	-1		*0*	*1*		
	D1NSI	D2SI	D2SI	D1NSI	D2SI	D1NSI
R_Q[a]	1.3	3	6.5	10	10	6.26
Q_T (ml/min)[b]	1	1	4.25	7.5	7.5	4.64

[a] Rq = Qas/Qdm
[b] Qt = Qas + Qdm

The experimental plan was also simulated using COMSOL® software. The values of the variables correspond to those used for D1NSI. For the simulations, Laminar Flow was used to solve the fluidic problem and Transport of Diluted Species physics was used for the convection and diffusion problem.

The main objectives of the simulation were: to verify flow focalization inside the NPC and its variations with R_Q and Q_T; to estimate the solvent diffusion profile in perpendicular planes to the NPC length and spaced every 0.5 mm

from the NPC start-point; to estimate the nanoprecipitation formation region taking into account the solvent diffusion profile and the materials' solubility parameters. At this time, only acetone diffusion into water has been simulated. The polymer and drug concentration effects on diffusion have not yet been taken into account.

(7) Calculation of Hansen Solubility Parameters

HSPs can be obtained from tables for several solvents and polymers, or calculated approximately if such tables are not available. A method used to calculate the parameters takes into account the contribution of the chemical functional group [9, 10, 33]. For the mixture of the components, the HSPs were obtained based on average weighting by component volume fraction [12].

As not all chemical component HSPs could be found, it was decided that they should all be calculated based on the chemical functional group contribution. The Hoy approach was used to determine the HSPs of Pluronic F127, PCL 80K and hydrocortisone acetate [9]. The acetone HSPs were calculated in accordance with the Van Krevelen data table and the procedure indicated in reference [7]. The HSPs used for water were selected from reference [8]. The calculated HSPs values are shown in Table 2. The HSPs of the water-acetate mixture were calculated by combining the corresponding parameters of the acetate and water multiplied by the volume fraction of each liquid.

Table 2: Calculated Hansen Solubility Parameters.

Chemical Compound	δ_d (MPa$^{1/2}$)	δ_p (MPa$^{1/2}$)	δ_h (MPa$^{1/2}$)	δ_v (MPa$^{1/2}$)
Pluronic F127	16.68	9.76	7.77	19.32
PCL 80K	16.10	11.45	9.04	19.76
Copolymer Block XVF127 = 0.82 XVPCL = 0.18	16.57	10.06	8	19.4
Hydrocortisone Acetate	13.68	12.77	12.85	18.71
Acetone	14.04	10.74	15.55	17.67
Water	15.5	16	42.3	22.28

X_{VF127} => Pluronic Volume Fraction
X_{VPCL} => PCL Volume Fraction

Bagley projected the Hansen three-dimensional space in a two-dimensional space by introducing the combined parameter δ_v [12, 34]. This parameter can be calculated according to Equation (1).

$$\delta = \sqrt{\delta_d^2 + \delta_p^2} \quad (1)$$

where
δ_d : dispersion solubility parameter,
δ_p : polar solubility parameter.

The parameter δ_h plotted versus δ_v leads to Bagley's Diagram. "It was found that good solvents must be included in the circle of a radius of five δ-units around the polymer" [12]. Bagley's diagram for the copolymer block, hydrocortisone acetate and water-acetone mixture is shown in Fig. 4. As shown in this figure, the water-acetone mixture is a good solvent for the copolymer block and hydrocortisone acetate up to 80 % and 67 % of the solvent volume fraction respectively. This is therefore the nanoparticle generation region for both compounds.

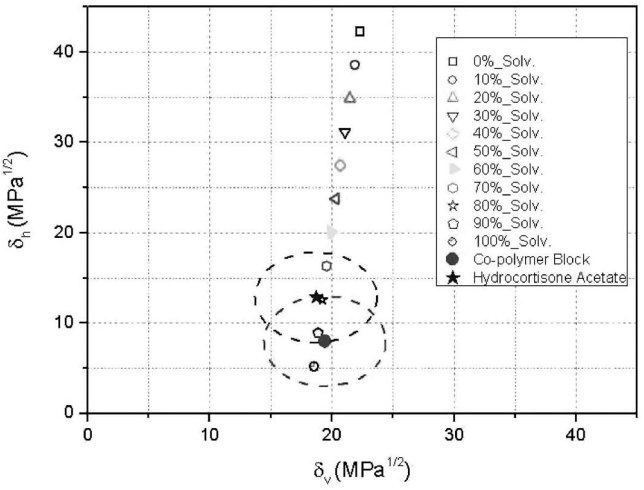

Fig. 4: Bagley's diagram for copolymer block, hydrocortisone acetate and water-acetate mixture (showing the acetate volume fraction). Dashed circles represent the five δ-units circle delimiting good solvents HSPs for copolymer block and hydrocortisone acetate.

(8) Simulation setup and analysis methodology

The simulations used the materials already defined in the COMSOL library, specifically the liquids water and acetone. For the Laminar Flow physics the fluids were considered incompressible and the temperature set to 20 °C. For each simulation, the Antisolvent Flow Rate (Q_{AS}) and the Organic Phase Flow Rate (Q_{DM}) values were calculated and defined as input values. For the AS inlets, the flow at every input was defined as indicated in Table 3 for D1NSI and as $Q_{AS}/4$ for D2SI. The output was set to 0 Pa. For the Transport of Diluted Species physics, the transport mechanism was set to convection. In the Convection and Diffusion node, the velocity field was used to connect both physics; water was used as bulk material and an isotropic diffusion coefficient of 1.16×10^{-9} m^2/s was specified. At the solvent input channel, the acetone concentration was fixed at 13619.35 mol/m^3.

Table 3: Antisolvent inlet flow

	Q_{AS} (ml/min)	Top inlet (ml/min)	Bottom inlet (ml/min)	Right inlet (ml/min)	Left inlet (ml/min)
Unbalanced Inputs	0.565	0.1	0.13	0.17	0.17
	0.909	0.16	0.2	0.27	0.27
	4.239	0.9	1.04	1.14	1.16
	6.818	1.56	1.72	1.77	1.78
	4	0.84	0.98	1.08	1.1
Balanced Inputs	Q_{AS}	$Q_{AS}/4$	$Q_{AS}/4$	$Q_{AS}/4$	$Q_{AS}/4$

Two different meshes, calibrated for fluids dynamics, were used for simulation of the devices. MESH1 defined

two different sizes, one for the body of the devices and another for input and output boundaries. A maximum and minimum element size of 100 µm and 30.6 µm, respectively, was used for the body. For the boundaries the element size was calibrated to Extremely Fine and the maximum element size was modified to 30 µm. MESH2 used just one size for the whole device, calibrated for Extremely Fine and its maximum element size was modified to 30 µm.

MESH1 was used to study the effect of balanced or unbalanced flow rate at AS inlets in D1NSI. MESH2 was used to study the diffusion process in D1NSI and D2SI.

A total of 14 planes were defined along the NPC and spaced every 0.5 mm. On each plane, the average concentration value (C_{avg}) was calculated as the integral of the concentration (C) in every node divided by the plane area. C is a COMSOL built-in variable.

The Relative Difference (RD) indicator was introduced to analyze possible diffusion-related differences between the devices. It was also used to analyze differences in D1NSI when working with unbalanced or balanced AS input flow rates. When used to compare devices, it was calculated according to Equation (2). For analysis of the differences in AS input flow rates, Equation (3) was used.

$$RD = \frac{100 \cdot |C_{avgD1NSI} - C_{D2SI}|}{C_{avgD1NSI}} \quad (2)$$

$$RD = \frac{100 \cdot |C_{avgD1NSI\text{-}UB} - C_{D1NSI\text{-}B}|}{C_{avgD1NSI\text{-}UB}} \quad (3)$$

where

$C_{avgD1NSI\text{-}UB}$: C_{avg} for D1NSI when working with unbalanced inputs.

$C_{avgD1NSI\text{-}B}$: C_{avg} for D1NSI when working with balanced inputs.

An already built-in variable (chds.c0avg_c_out1) was used to obtain the concentration at the output boundary (C_{out}).

The indicator Diffusion Stage (DS) was introduced for monitoring the diffusion process. DS is calculated according to Equation (4). For a fully developed diffusion process, the C_{avg} equals the C_{out} and DS = 1.

$$DS = \frac{C_{avg}}{C_{out}} \quad (4)$$

The acetone volume fraction (X_{Vact}) was calculated as in Equation (5). This data, in conjunction with Bagley's diagram information, was employed for estimating the nanoparticle generation region.

$$X_{Vact} = \frac{C \cdot MM_{act}}{\rho_{act}} \quad (5)$$

where

MM_{act}: acetone molar mass,

ϱ_{act}: acetone density (built-in property).

IV. Results and Discussion

(1) Simulations results

To obtain 45° input channels in the vertical direction, we had to design Stair-Like Channels (SLC) owing to fabrication constraints. This type of channel experiences a variable Hydraulic Resistance (R_H), which is dependent on the flow rate. Two input channel sections, Practically Straight Channel (PSC) and SLC (horizontal and vertical directions respectively), Figs. 5a and 5b, were simulated to understand how the flow rate distribution is affected by R_H. Fig. 5c shows the Pressure vs Flow Rate graph for both channel topologies. Non-linear behavior can be seen for the SLC. The simulated flow rate varied from 0.1875 ml/min to 1.705 ml/min. Owing to the nonlinearity, the R_H, which is the P vs Q slope, is not constant. The R_H was obtained by calculating the P vs Q derivative, and the result was plotted versus the flow rate, Fig. 5d. The R_H for PSC is less sensitive to flow variations than the R_H for SLC.

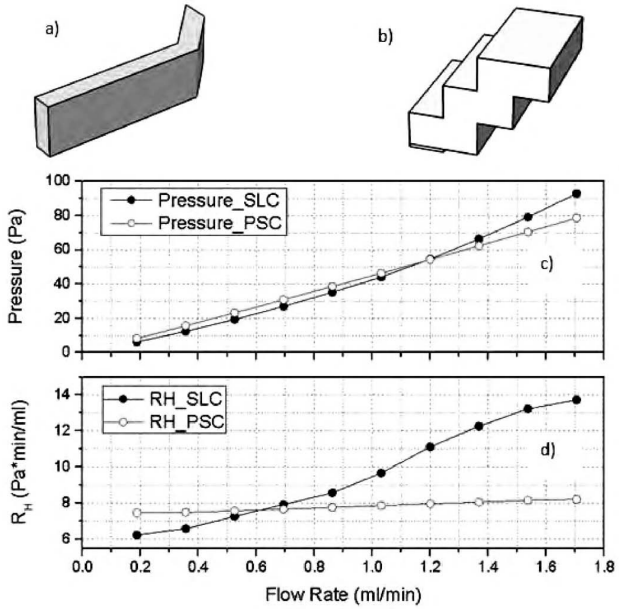

Fig. 5: Hydraulic resistance simulation results for the AS inlets. a) Practically Straight Channel. b) Stair-Like Channel. c) Pressure vs Flow Rate graph. It is possible to see the nonlinear behavior for SLC. d) Hydraulic Resistance vs Flow Rate. Due to the nonlinear relationship, R_H increases with increasing flow rate.

These simulation results indicate that as the total AS flow rate increases the SLC R_H increases as well, reducing the flow rate. PSC has an almost constant R_H. The differences in R_H lead to AS input flow rate asymmetries in the horizontal and vertical directions for the D1NSI device. The same does not happen in D2SI owing to the balanced R_H of its input channels. The main microfluidic-related difference between the two devices can be seen in Fig. 6. For higher R_Q and Q_T values, the focalized stream loses its almost cylindrical flow profile in D1NSI, Figs. 6b and 6d. This is due to the force asymmetries; the force in the horizontal direction is higher than that in the vertical direction.

The focalized organic phase dissolved material stream in the NPC center for D1NSI and D2SI devices is shown in Fig. 7. As expected, antisolvent flow force action ensured an organic phase DM focalized stream owing to the inlet topology. As the R_Q value increases, the focalized stream diameter and organic phase concentration decreases. As can be seen in Fig. 6, the stream diameter reduction is helpful for the solvent diffusion and hence in the formation of super saturation regions for nanoparticle generation.

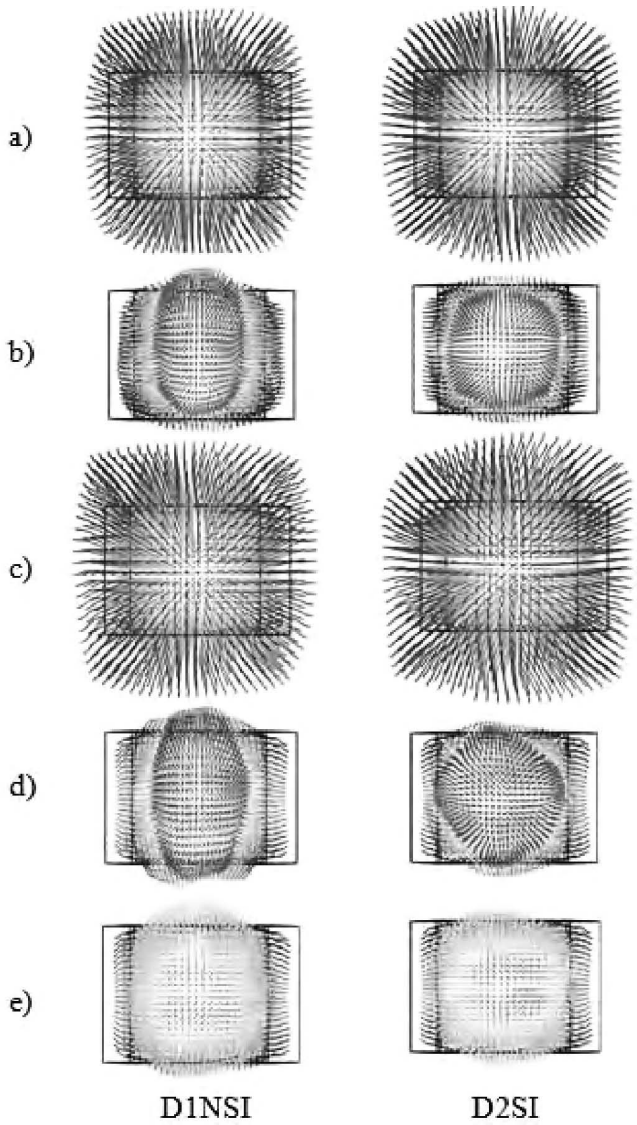

Fig. 6: Effect of the non-symmetrical AS input flow rates on the focalized stream. Shown are the velocity streamlines coming from the DM input. Unbalanced AS inlets flow rates were used for this simulation. a) R_Q = 1.3 and Q_T = 1 ml/min; b) R_Q = 10 and Q_T = 1 ml/min; c) R_Q = 1.3 and Q_T = 7.5 ml/min; d) R_Q = 10 and Q_T = 7.5 ml/min; e) R_Q = 6.26 and Q_T = 4.64 ml/min.

The D1NSI device showed no difference in the diffusion process when working with unbalanced and balanced AS inlet flow rates, as can be seen in Fig. 8a. The Relative Difference was lower than 1.5 % along the NPC. No differences were observed in the diffusion process when D1NSI and D2SI were simulated, Fig. 8b. Along the NPC, the relative difference in the average concentration was lower than 2.5 %. The results showed no effect of the input channel topologies on the diffusion process for the used flow rate parameters.

The diffusion process evolution along the NPC can be seen in Fig. 9. The maximum Diffusion Stage indicator value attained by the two devices was 85 %, Fig. 9a. This means that, at the output, the solvent was not fully diffused. In Fig. 9b, it is possible to see remaining regions with lower solvent concentration in the NPC perimeter. If a fully developed diffusion process is required, then a longer NPC must be used.

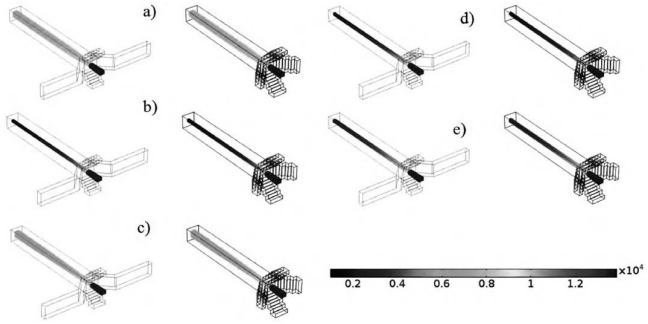

Fig. 7: 3D focalization inside D1NSI and D2SI devices. Color bar is Organic phase (DM) concentration in x 10^4 mol/m^3. a) R_Q = 1.3 and Q_T = 1 ml/min; b) R_Q = 10 and Q_T = 1 ml/min; c) R_Q = 1.3 and Q_T = 7.5 ml/min; d) R_Q = 10 and Q_T = 7.5 ml/min; e) R_Q = 6.26 and Q_T = 4.64 ml/min.

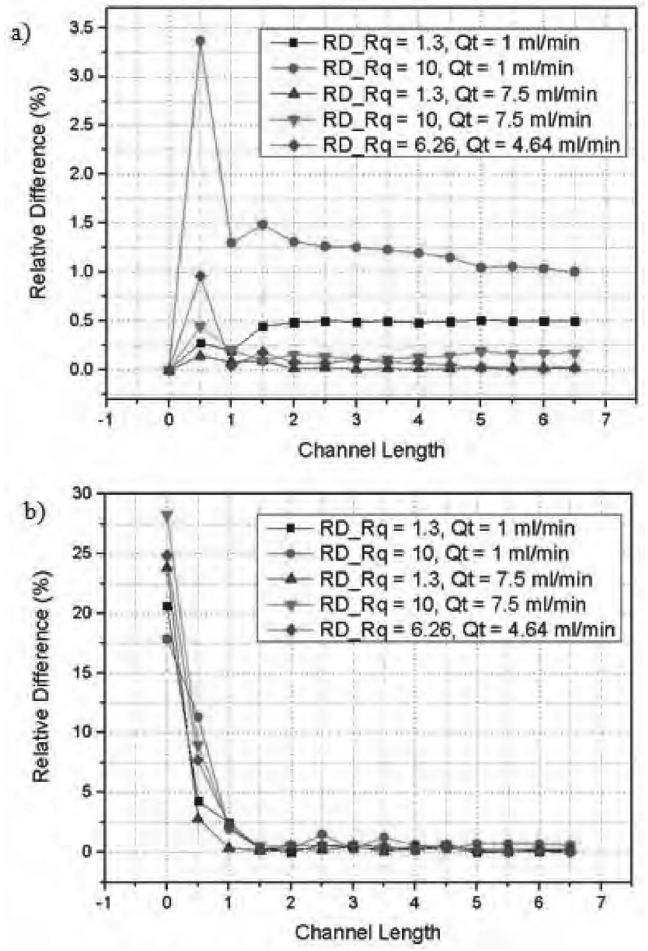

Fig. 8: Relative Difference for devices D1NSI and D2SI. a) RD for D1NSI when working with balanced and unbalanced AS inlets flow rate, calculated as in Equation (3). b) RD between D1NSI and D2SI when working with balanced AS inlets flow rate, calculated as in Equation (2).

For estimation of the nanoparticle generation region, a horizontal plane was created at the NPC half height. The acetone volume fraction was plotted in this plane. As the previous results showed no difference between the devices for the diffusion process, at this point just D2SI was analyzed. Fig. 10 shows the acetone volume fraction evolution in the device for different process conditions. Black and white lines indicate X_{Vact} = 0.67 and X_{Vact} = 0.8, delimit-

ing the nanoparticle generation region for hydrocortisone acetate and co-polymer block respectively, as showed in Bagley's diagram, Fig. 4. The regions inside the black or white lines have enough solvent concentration to maintain dissolution of the corresponding materials.

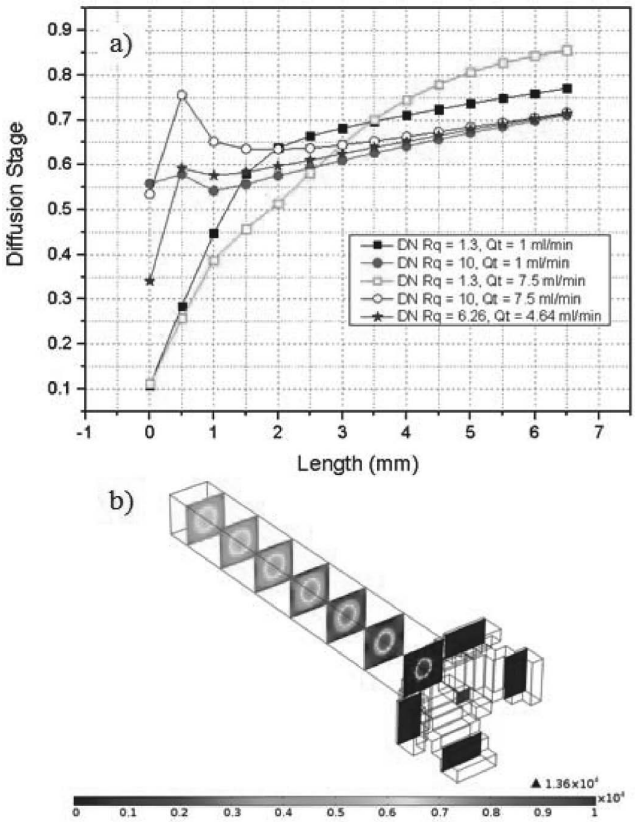

Fig. 9: Diffusion Stage calculated as in Equation (4). a) Results showed an antisolvent material not fully diffused in the NPC cross-section. The best DS obtained was 85 %. b) Diffusion evolution along NPC for R_Q = 1.3 and Q_T = 7.5 ml/min. Color bar in units of x10^4 mol/m^3.

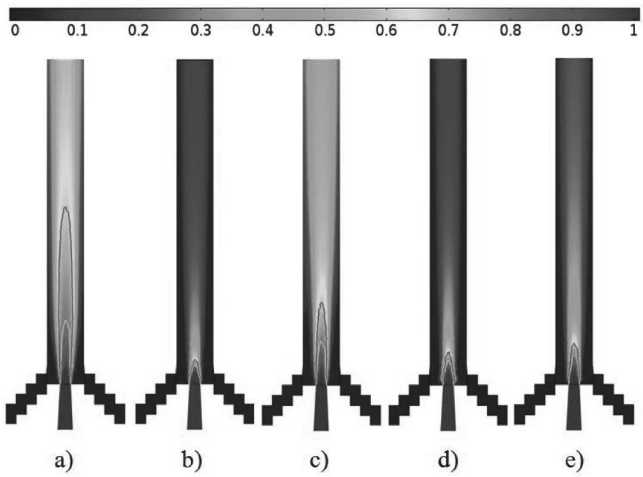

Fig. 10: Nanoparticles generation regions. Black and white lines indicate X_{Vact} = 0.67 and X_{Vact} = 0.8, delimiting the nanoparticles generation region for hydrocortisone acetate and co-polymer block respectively. a) R_Q = 1.3 and Q_T = 1 ml/min; b) R_Q = 10 and Q_T = 1 ml/min; c) R_Q = 1.3 and Q_T = 7.5 ml/min; d) R_Q = 10 and Q_T = 7.5 ml/min; e) R_Q = 6.26 and Q_T = 4.64 ml/min. The color bar denotes the acetone volume fraction.

Simulation results show that, even when the acetone diffusion process is not completely finished, the nanoparticle generation remains in the device domain.

For lower R_Q and Q_T values, the nanoparticle generation regions for hydrocortisone acetate and the co-polymer block are far apart. This could lead to a poor drug encapsulation because the co-polymer block nanoparticles will be generated before the drug nanoparticles.

For higher R_Q and Q_T values, the nanoparticle generation regions are closer for the two materials, suggesting an improved encapsulation process. For the same conditions, the nanoprecipitation process finishes close to the NPC beginning.

(2) Experimental results

Proposed factorial experimental planning results are summarized in Table 4.

		D1NSI		D2SI	
Rq	**Q_T (ml/min)**	**Tp (nm)**	**PDI**	**Tp (nm)**	**PDI**
1.3	1	459.1	0.235		
3	1			310.6	0.205
10	1	287.8	0.228	250.3	0.165
1.3	7.5	355.5	0.206		
3	7.5			277.5	0.196
10	7.5	188.9	0.102	162.2	0.131
6.26	4.64	233.4	0.188		
6.5	4.25			176.2	0.131
6.5	4.25			202.9	0.135
6.5	4.25			182.3	0.18

Results showed submicron and nanoparticles with sizes ranging from 188.9 nm to 459.1 nm for D1NSI and from 162.2 nm to 310.6 nm for D2SI. The polydispersity index remains lower than 0.235, which implies a narrow particle size distribution. Fig. 11 shows the Zetasizer Nano-ZS measurement for R_Q = 10 and Q_T = 7.5 ml/min and D1NSI.

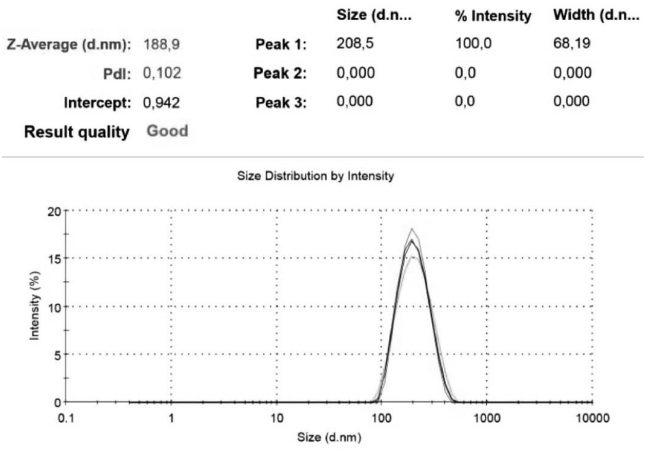

Fig. 11: Zetasizer Nano-ZS measurement for R_Q = 10 and Q_T = 7.5 ml/min (D1NSI).

The data obtained was analyzed with Statistica12 software in order to obtain a better representation of the influence of the process variables on the particle size (T_P) and polydispersity index (PDI). Figs. 12a and 12b shows the Pareto Chart for T_P and PDI respectively. Both process variables showed an inversely proportional relationship with T_P and PDI. The particle size showed a stronger dependence on the R_Q process variable, Fig. 12a. In turn, the polydispersity index showed a stronger dependence on the Q_T process variable, Fig. 12b.

The experimental data in Table 4 were rearranged from the lowest R_Q value to the highest. For the same R_Q value, the data were organized from the lowest Q_T value to the highest. For D2SI, the values for the repeated process conditions (central point) results were averaged and plotted, obtaining T_P = 187.13 nm and PDI = 0.149. The arranged data were plotted with a 3D trajectory graph. The results are shown in Fig. 13a (T_P) and Fig. 13b (PDI) for D1NSI, and Fig. 14a (T_P) and Fig. 14b (PDI) for D2SI. As shown by the Pareto Chart (Fig. 12), it can be seen that an increase in R_Q implies a decrease in T_P and PDI. The same applies for an increase in Q_T. These dependences show the system ability to tune the nanocapsule sizes. Variables R_Q and Q_T could be used for coarse- and fine-tuning, respectively.

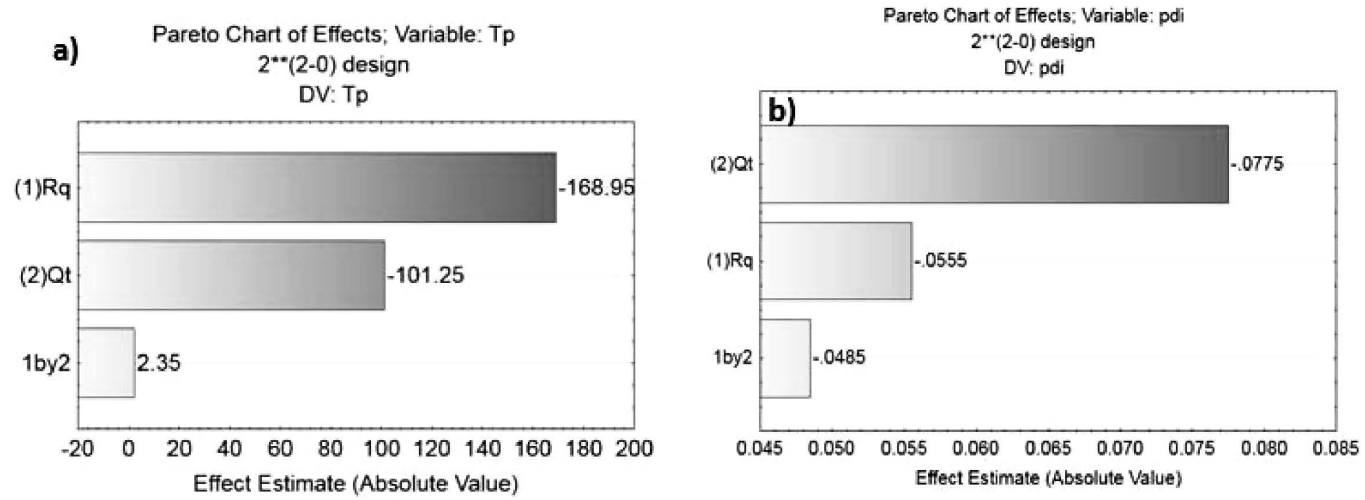

Fig. 12: Pareto Chart. a) Influence of process variables on the particle size; b) Influence of process variables on the polydispersity index.

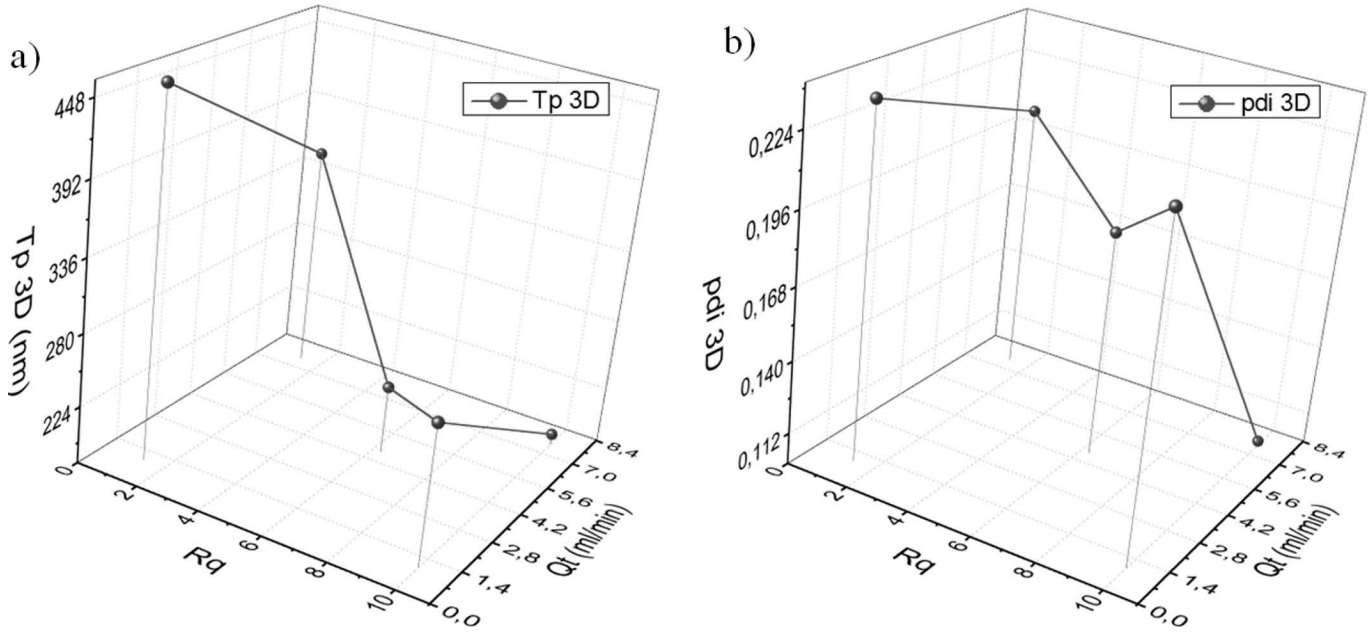

Fig. 13: 3D trajectory graph for D1NSI. a) Tp versus Rq and Q_T; b) PDI versus R_Q and Q_T.

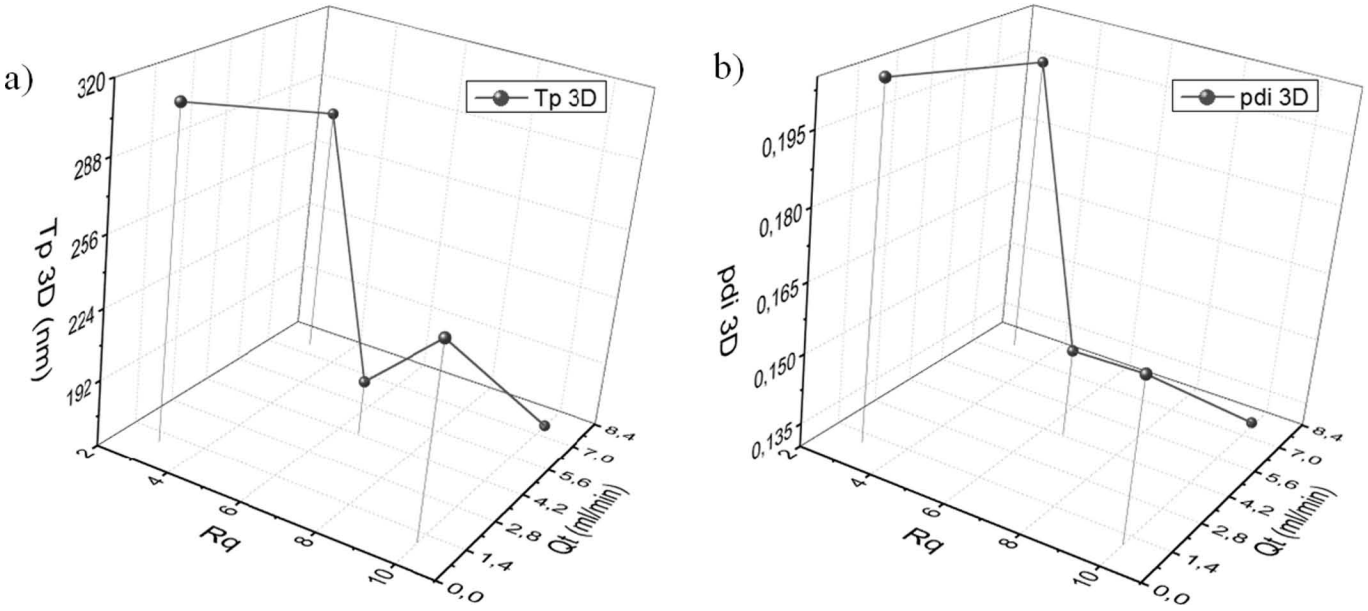

Fig. 14: 3D trajectory graph for D2SI. a) Tp versus Rq and Q_T; b) PDI versus R_Q and Q_T.

A deeper process product analysis will be conducted in future work in order to evaluate the encapsulation efficiency.

V. Conclusions

This work presents two 3D flow focalization microfluidic devices manufactured with LTCC technology for the production of nanocapsules. The working principle of these devices is the nanoprecipitation process.

Inlet channel topology with suitable 45° inclination in the vertical and horizontal directions ensures full 3D flow focalization.

The main difference between the two devices is the antisolvent inlet topology. Device D1NSI has two stair-like channels to ensure the 45° inclination in the vertical direction while using practically straight channels in the horizontal direction. Device D2SI has the four antisolvent input channels with stair-like channel topology.

Simulation shows no differences between the devices for the diffusion process. The main difference between the two devices it is that the focalized stream of the asymmetric one deforms at higher values for the flow rate ratio.

Simulations indicate co-polymer and drug nanoprecipitation regions could be far apart from each other for a low flow rate ratio and total flow, suggesting poor drug encapsulation. This can be overcome by increasing the flow rate ratio and total flow rate through the device, leading to devices with a higher production rate.

This work reports monomodal submicron particle and nanoparticle production with Zetasizer-measured sizes ranging from 188.9 nm to 459.1 nm and from 162.2 nm to 310.6 nm for devices D1NSI and D2SI respectively. The polydispersity index varies from 0.102 to 0.235 and from 0.131 to 0.205 for devices D1NSI and D2SI respectively. This is a work in progress. Other experiments will be repeated in triplicate for verification of statistical data consistency.

Clearly shown in the possibility of using the process variables R_Q and Q_T for coarse- and fine-tuning of the nanocapsule size. This work presents devices working at up to 7.5 ml/min, which is two orders of magnitude higher than the flow rates reported in the literature.

Acknowledgements

We acknowledge FINEP contract N°01.11.0108.00 for financial support.

We thank Andre Luiz Nunis da Silva from the Institute for Technological Research for use of the COMSOL software to perform the simulations.

HCG wishes to acknowledge "Coordenação de Aperfeiçoamento de Pessoal de Nível Superior", CAPES for financial support.

References

1 Stainmesse, S., Orecchioni, A.M., Nakache, E., Puisieux, F., Fessi, H.: Formation and stabilization of a biodegradable polymeric colloidal suspension of nanoparticles, *Colloid. Polym. Sci.*, **273**, 505 – 511, (1995).

2 Nagavarma, B.V.N., Yadav, H.K.S., Ayaz, A., Vasudha, L.S., Shivakumar, H.G.: Different techniques for preparation of polymeric nanoparticles – A review, *Asian J. Pharm. Clin. Res.*, **5**, 16 – 23, (2012).

3 Chen, H., Khemtong, C., Yang, X., Chang, S., Gao, J.: Nanonization strategies for poorly water-soluble drugs, *Drug Discov. Today*, **16**, 354 – 360, (2011).

4 Schubert, S., Delaney Jr, J.T., Schubert, U.S.: Nanoprecipitation and nanoformulation of polymers: From history to powerful possibilities beyond poly(lactic acid), *Soft Matter*, **7**, 1581 – 1588, (2011).

5 Lepeltier, E., Bourgaux, C., Couvreur, P.: Nanoprecipitation and the "Ouzo effect": Application to drug delivery devices, *Adv. Drug Deliv. Rev.*, **71**, 86 – 97, (2014).

6 Chan, H.K., Kwok, P.C.L.: Production methods for nanodrug particles using the bottom-up approach, *Adv. Drug Deliv. Rev.*, **63**, 406 – 416, (2011).

[7] Barton, A.F.M.: CRC Handbook of solubility parameters and other cohesion parameters, Second Edition: Taylor & Francis, 1991.

[8] Hansen C.M.: Hansen solubility parameters: A user's handbook, Second Edition ed.: CRC Press, 2007.

[9] van Krevelen, D.W.: Properties of polymers: Elsevier Science, 2012.

[10] van Krevelen, D.W., te Nijenhuis, K.: Properties of polymers: Their correlation with chemical structure; their numerical estimation and prediction from additive group contributions: Elsevier Science, 2009.

[11] Wang, S.H., Liu, J.H., Pai, C.T., Chen, W., Chung, P.T., Chiang, A.S.T., Chang, S.J.: Hansen solubility parameter analysis on the dispersion of zirconia nanocrystals, *J. Colloid Interf. Sci.*, **407**, 140 – 147, (2013).

[12] Othman, R., Vladisavljević, G.T., Hemaka Bandulasena, H.C., Nagy, Z.K.: Production of polymeric nanoparticles by micromixing in a co-flow microfluidic glass capillary device, *Chem. Eng. J.*, **280**, 316 – 329, (2015).

[13] Ali, H.S.M., Blagden, N., York, P., Amani, A., Brook, T.: Artificial neural networks modelling the prednisolone nanoprecipitation in microfluidic reactors, *Eur. J. Pharm. Sci.*, **37**, 514 – 522, (2009).

[14] Ali, H.S.M., York, P., Ali, A.M.A., Blagden, N.: Hydrocortisone nanosuspensions for ophthalmic delivery: A comparative study between microfluidic nanoprecipitation and wet milling, *J. Control. Release*, **149**, 175 – 181, (2011).

[15] Wang, J.X., Zhang, Q.X., Zhou, Y., Shao, L., Chen, J.F.: Microfluidic synthesis of amorphous cefuroxime axetil nanoparticles with size-dependent and enhanced dissolution rate, *Chem. Eng. J.*, **162**, 844 – 851, (2010).

[16] Ali, H.S.M., York, P., Blagden, N.: Preparation of hydrocortisone nanosuspension through a bottom-up nanoprecipitation technique using microfluidic reactors, *Int. J. Pharma.*, **375**, 107 – 113, (2009).

[17] Aghajani, M., Shahverdi, A.R., Amani, A.: The use of artificial neural networks for optimizing polydispersity index (PDI) in nanoprecipitation process of acetaminophen in microfluidic devices, *AAPS PharmSciTech*, **13**, 1293 – 1301, (2012).

[18] Karnik, R., Gu, F., Basto, P., Cannizzaro, C., Dean, L., Kyei-Manu, W., Langer, R., Farokhzad, O.C.: Microfluidic platform for controlled synthesis of polymeric nanoparticles, *Nano Lett.*, **8**, 2906 – 2912, (2008).

[19] Valencia, P., Basto, P., Gu, F., Zhang, L., Cannizzaro, C., Langer, R., Farokhzad, O., Karnik, R.: Novel synthesis of polymeric nanoparticles for drug delivery applications using microfluidic rapid mixing, in 12th International Conference on Miniaturized Systems for Chemistry and Life Sciences, MicroTAS 2008, San Diego, CA, 2008, 1513 – 1515.

[20] Schianti, J.N., Cerize, N.N.P., de Oliveira, A.M., Derenzo, S., Seabra, A.C., Góngora-Rubio, M.R.: Rifampicin nanoprecipitation using flow focusing microfluidic device, *J. Nanomed.Nanotechnol.*, **4**, (2013).

[21] Capretto, L., Cheng, W., Carugo, D., Katsamenis, O.L., Hill, M., Zhang, X.: Mechanism of co-nanoprecipitation of organic actives and block copolymers in a microfluidic environment, *Nanotechnology*, **23**, (2012).

[22] Capretto, L., Carugo, D., Cheng, W., Hill, M., Zhang, X.: Continuous-flow production of polymeric micelles in microreactors: experimental and computational analysis, *J. Colloid Interf. Sci.*, **357**, 243 – 251, (2011).

[23] Cobas Gomez, H., Seabra, A.C., Araujo Feitosa, V., de Novais Schianti, J., Marim de Oliveira, A., Wasnievski da Silva de Luca Ramos, L., Gongora-Rubio, M. R.: Development of a LTCC micro spray dryer, in sensors (IBERSENSOR), 2014 IEEE 9th Ibero-American Congress on, 2014, 1 – 5.

[24] Rhee, M., Valencia, P.M., Rodriguez, M.I., Langer, R.S., Farokhzad, O.C., Karnik, R.: 3D hydrodynamic focusing for confined precipitation of nanoparticles within microfluidic channels, in 14th International Conference on Miniaturized Systems for Chemistry and Life Sciences 2010, MicroTAS 2010, Groningen, 2010, 992 – 994.

[25] Rhee, M., Valencia, P.M., Rodriguez, M.I., Langer, R., Farokhzad, O.C., Karnik, R.: Synthesis of size-tunable polymeric nanoparticles enabled by 3D hydrodynamic flow focusing in single-layer microchannels, *Adv. Mater.*, **23**, H79 – H83, (2011).

[26] Schianti, J.N., Cerize, N.P.N., Oliveira, A.M., Derenzo, S., Góngora-Rubio, M.R.: 3-D LTCC microfluidic device as a tool for studying nanoprecipitation, 8th Ibero-American Congress on Sensors, IBERSENSOR 2012, vol. 421, 2013.

[27] Lim, J.M., Bertrand, N., Valencia, P.M., Rhee, M., Langer, R., Jon, S., Farokhzad, O.C., Karnik, R.: Parallel microfluidic synthesis of size-tunable polymeric nanoparticles using 3D flow focusing towards *in vivo* study, *Nanomedicine: NBM*, **10**, 401 – 409, (2014).

[28] Gongora-Rubio, M.R., Schianti, J.d.N., Cobas, H., Teves, A. d. C.: LTCC-3D coaxial flow focusing microfluidic reactor for micro and nanoparticle fabrication and production scale-out, *Journal of Microelectronic & Electronic Packaging*, **10**, (2013).

[29] Gongora-Rubio, M.R., Espinoza-Vallejos, P., Sola-Laguna, L., Santiago-Avilés, J.J.: Overview of low temperature co-fired ceramics tape technology for meso-system technology (MsST), *Sensor. Actuat. A.-Phys*, **89**, 222 – 241, (2001).

[30] Dias, A.R.M.: Síntese e caracterização de copolímeros em bloco anfifílicos, por transesterificação, com redução de massa molar da poli(ε-caprolactona), Master, Instituto de Pesquisas Tecnológicas do Estado de São Paulo, São Paulo, 2015.

[31] Harvard_Apparatus, "PHD 4400 Hpsi. High Force/High Pressure Programmable Syringe Pump," Harvard Apparatus.

[32] Neto, B.B., Scarminio, I.S.,Bruns, R.E.: Como fazer experimentos, 4ta ed., *Bookman*, 2010.

[33] Eliche, E.B.: Sistemas dispersos tópicos de lidocaína base en solución, PhD, Departamento de Farmacia y Tecnología Farmacéutica, Universidad de Granada, Granada, 2010.

[34] Thakral, S. Thakral, N.K.: Prediction of drug-polymer miscibility through the use of solubility parameter based flory-huggins interaction parameter and the experimental validation: PEG as model polymer, *J. Pharm. Sci.*, **102**, 2254 – 2263, (2013).